Tampere University

Iisa Aromäki

Ag NANOPARTICLES IN TELLURITE GLASSES

Faculty of Engineering and
Natural Sciences
Bachelor of Science Thesis
September 2021

ABSTRACT

Iisa Aromäki: Ag nanoparticles in tellurite glasses
Bachelor of Science Thesis
Tampere University
Bachelor's Programme in Engineering and Natural Sciences
September 2021

The objective of this project was to investigate the effect of addition of Ag_2O on the spectroscopic properties of tellurite glasses and examine if silver nanoparticles can be grown in such glasses to enhance their spectroscopic properties. First, the impact of silver oxide concentration on the glass network was studied, and then the effect of heat-treatment duration on the growth of the silver nanoparticles was investigated.

Glasses with the composition (100-x-y) ($70TeO_2$-$20ZnO$-$10Bi_2O_3$)-xAg_2O-yEr_2O_3 with x = 0, 0.5, 1, 2 and 4 and y = 0 and 2.5 in mol% were prepared using the conventional melting quenching method. Afterwards glasses were heat-treated at T_g + 20 °C for 2, 5 and 17 hours to eventually grow the silver nanoparticles.

The progressive addition of Ag_2O was found to modify the thermal and spectroscopic properties of the glass, increasing the thermal stability against crystallization due to the depolymerization of the tellurite network. However, even though the addition of Ag_2O modified the glass network, it did not change the site of Er^{3+}-ions. However, the highly Ag containing glasses exhibit lower intensity of upconversion when pumped at 980 nm suggesting that the Er-Er distance increases when adding Ag_2O probably due to the depolymerization of the tellurite network.

A heat-treatment of the glasses at their T_g + 20 °C changed their color and their transparency due to crystallization, which was confirmed using XRD. The XRD pattern of the heat-treated glass exhibit similar sharp peaks which belong to the Bi_4TeO_8 crystals. In the XRD pattern and absorption spectra of the heat-treated glasses, there was no evidence of the precipitation of silver nanoparticles occurring during the heat-treatment. Additionally, the shapes of the Er^{3+} emission spectra remained similar after heat-treatment indicating that the Er^{3+} ions remained in the amorphous part of glass. However, the intensity of the conversion was found to increase after heat-treatment only in the low Ag containing glasses suggesting that the Er-Er distance decreases in the polymerized glasses due to the precipitation of Bi_4TeO_8 crystals. In the depolymerized network, the Er-Er distance does not seem to be impacted by the precipitation of Bi_4TeO_8 crystals.

Keywords: Tellurite glass, rare-earth ions, silver nanoparticles, laser glass

PREFACE

This thesis was made as a part of a Bachelor's Programme in Engineering and Natural Sciences at Tampere University. The research was done in the Photonic Glasses research group under the supervision of Laeticia Petit in the Laboratory of Photonics. The experiments were mostly done during summer 2021.

For very first, I would like to thank Professor Laeticia Petit for her guidance and help during my summer. Also, I would like to thank Reynald Ponte for his support and help with experiments as well as processing the collected data. And I would like to thank all my lab mates for their help and advice.

Tampere, 23 September 2021

Iisa Aromäki

CONTENTS

LIST OF FIGURES

LIST OF SYMBOLS AND ABBREVIATIONS

θ	Diffraction angle
A	Absorption
c	speed of light
d	Distance between atom planes
E	Energy
F_b	Buoyance force
g	Standard acceleration of freefall
h	Planck constant
I	Intensity
l	Thickness of glass sample
m	Mass
N	Ion concentration
n	Integer
T	Temperature
ΔT	Temperature difference
V	Volume
α	Absorption coefficient
σ	Absorption cross-section
λ	Wavelength
ρ	Density
°C	Celsius Degrees (0 °C = 273.15 K)
g	Gram (1 g = 10^{-3} kg)
cm	Centimeter (1 cm = 10^{-2} m)
µm	Micrometer (1 μ = 10^{-6} m)
nm	Nanometer (1 nm = 10^{-9} m)
h	Hour (1 h = 3600 s)
min	Minute (1 min = 60 s)
s	Second
a.u.	Arbitrary Unit
AD	Anno Domino
DC	Downconversion
DSC	Differential Scanning Calorimeter
ESA	Excited-state absorption
ET	Energy transfer
ETU	Energy-transfer upconversion
GSA	Ground state absorption
HT	Heat-treatment
IR	Infrared
LFE	Local field enhancement
mol%	mole present
NP	Nanoparticle
PA	Photon avalanche
Pt	Platinum
RE	Rare-earth
SPR	Surface plasmon resonance
T_g	Glass transition temperature
T_m	Glass melting temperature
T_p	Crystallization peak temperature
T_x	Crystallization onset temperature
UC	Upconversion

UV-Vis-NIR	Ultraviolet-Visible-Near Infrared
XRD	X-Ray Diffraction
Ag	Silver
Ag_2O	Silver oxide
Ag_2SO_4	Silver(I) sulfate
Bi_2O_3	Bismuth(III) oxide
Er_2O_3	Erbium(III) oxide
Er^{3+}	Erbium ion
Te	Tellurium
TeO	Tellurite oxide
ZnO	Zinc oxide

1. INTRODUCTION

The superfast revolution of information technology in the last years would not have happened without the advanced photonic applications and knowledge behind them. Photonics is an area of optics and it concentrates on the use of light. Photonics separated from optics in the 1960s after the invention of the laser. (Synopsys, 2021) Nowadays, photonics has a wide range of applications. On top of the optical fibers and telecommunication, photonics' applications are diverse, going from cell phone cameras to the medical field (Synopsys, 2021). The evolution and development of new photonic devices demand new photonic materials, which is a very important area to study.

Glass is a very suitable host material for optical applications because it can be embedded with rare-earth ions (L. Liu, 2018). Glass provides a sufficient and stable environment for them. Tellurite glass has especially attracted much interest lately due to its promising properties such as lower phonon energy and melting temperature compared to the well-known silica glass (H. Fares I. J., 2014). Recently, it was found that metallic nanoparticles can enhance the spectroscopic properties glasses doped with rare-earth elements (J. Qi 2013).

This thesis has two main objectives. The first one is to investigate the impact of the addition of Ag_2O on the various properties of tellurite glasses, and the second is to investigate if it is possible to grow silver nanoparticles in glass using heat to enhance the spectroscopic properties of the glass.

The brief theory behind this study is discussed in chapter 2. It provides information about glasses, glass formation, tellurite glasses, the lasing principle of glasses, and the state of the art on the development of Ag nanoparticles in Er^{3+} doped glasses.

In chapter 3, the preparation and characterization methods of the investigated glasses are summarized. DSC, Raman spectroscopy, XRD, and density measurements are used to study the glass thermal, structural, and physical properties. Furthermore, absorption and luminescence measurements are carried out to study the optical and spectroscopic properties.

The results are presented in chapter 4. In addition, the chapter includes further discussion about the measured data. And this thesis ends with a conclusion and discussion about the next steps in chapter 5.

2. BACKGROUND

2.1 Glasses

Glass is one of the oldest and widest-used materials. The first man-made glasses have been fabricated as early as 3500 AD (Nissink Business Glass n.d.). Originally, glasses were made with a soda-lime-silica composition, and even today most of the glasses are silica-based (Britannica n.d.). For instance, silica glasses can be found in windows, drinking glasses, and glass bottles. However, during past centuries, new glass compositions have been developed and now, a high number of different glasses exists. By changing the fabrication method or the chemical components of the glass, its properties, such as hardness, transparency, and viscosity, can be modified to suit the best to the purpose the glass is prepared for.

2.1.1 Glass formation

Even though glasses with different compositions can have various properties, still all of them have two common characteristics: first, the structure of all glasses is amorphous, contrary to any crystalline material. The arrangement of the atoms possesses no periodicity, meaning that they do not exhibit any long-range order. Second, a glass is formed from a seemingly supercooled liquid state over a controlled range of temperatures called “glass transformation range”. (Shelby 2005) A schematic diagram of the glass formation is presented in Figure 1.

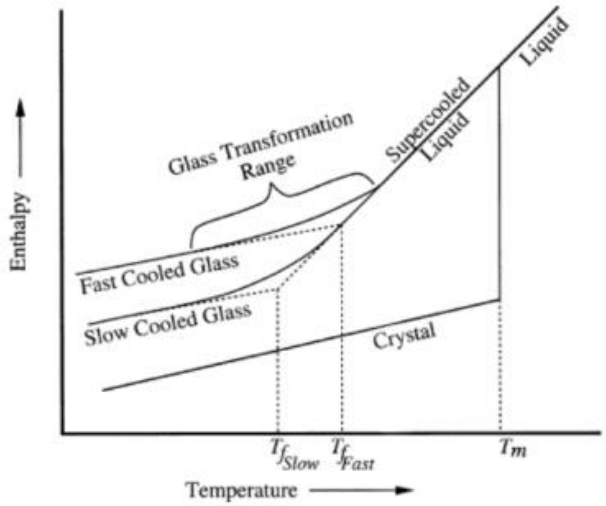

Figure 1: Schematic diagram of the formation of glass. (Shelby 2005)

As can be seen in Figure 1, below the glass melting temperature T_m, a glass, can create crystals or stay as a supercooled liquid when cooling down.

- If crystals are formed, enthalpy is released, and a periodic atomic structure forms. Consequently, the material cannot be considered as a glass anymore. (Shelby 2005)
- If a glass melt is cooled down below the melting temperature without crystallization, then the melted state is called a supercooled liquid. The viscosity of this liquid increases when the temperature of the supercooled liquid decreases. While the viscosity increases, it becomes harder and harder for atoms to rearrange to a periodic structure. In that case, the structure remains amorphous, and a glass is formed.

Figure 1 also shows that the enthalpy of the glass depends on a cooling rate, and therefore the structure of a glass, also depends on the thermal history of preparation of the glass (Shelby 2005).

2.1.2 Tellurite glasses

Rather new and interesting alternative glasses to silica glass are the tellurite glasses. Their properties have been studied extensively, and they have shown many promising qualities/assets. Tellurite glasses have high transmittance window from near (NIR) to middle infrared (MIR) region, good thermal and chemical stabilities, and high linear and non-linear refractive indices. (H. E. H. Fares 2014) Thus, they are good candidates for optical fiber drawing, laser devices, non-linear optical devices, and fast optical switches. (I. Jlassi 2011) (W. Stambouli 2012)

Properties, which make tellurite glass attractive material for this study, are their high rare-earth (RE) ion solubility and lower phonon energy than many common glasses, such as silicates and phosphates glasses. When the environment around RE ions has low phonon energy, then non-radiative losses are minimized, and therefore higher efficiency can be reached. (I. J. H. Fares 2014) On top of that, tellurite glasses have a relatively low melting temperature, which make them easier and cheaper to fabricate compared to silica glass for example (N.M. Yusoff 2015).

In the basic network of tellurite glass, TeO_4 units are in a shape of a bipyramid, and one unit is connected to the other via Te-O-Te linkages as shown below in Figure 2.

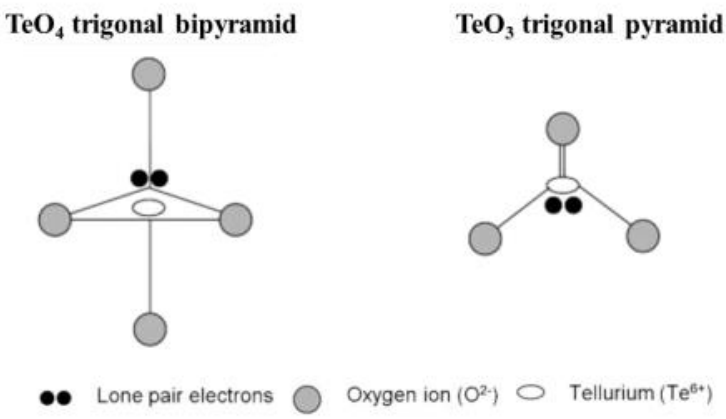

Figure 2: Schematic of the structural units in the tellurite glass, modified from (A. Jha 2012) TeO_4 and TeO_3 units can be labeled also as Q^4 and Q^3 respectively according to the number of bridging oxygens.

One should mention that tellurite oxide does not form stable glass by itself due to the lonely electron pairs in TeO_4 units, which set limits to the glass network and, therefore the preparation of glass (I. J. H. Fares 2014). To create TeO_2 glass, one way is to use certain fixed conditions, such as a very high cooling rate. Another alternative is to add metal oxides, for example, Na_2O, BaO, ZnO, WO_3, to the glass system. Metal oxides are considered to be glass modifiers or intermediates since they break chains of the structural units, modify the glass network and therefore improve the glass formation ability. When a metal oxide is added into the glass matrix, part of TeO_4 units is reformed into more disordered TeO_{3+1} and TeO_3 units (see Figure 2). (A. Kaur 2010)

2.2 Lasing glasses

Doping a glass with RE ions makes it optically active. The lanthanide series, scandium (Sc), and yttrium (Y) form the rare-earth ions, and they are known as luminescence centers in glasses. Due to its high rare-earth ion solubility, synthesizing flexibility, and inhomogeneous line broadening of the RE ions emission, glass can be a great host for rare-earth ions (L. Liu 2018).

Lasing properties of RE doped glasses is based on rare-earth ions specific electron configuration. At the same time, the configuration allows electron transitions in the 4f shell, and ion outer electron shells shield the 4f shell from the surrounding environment. (M. Kemere 2017)

2.2.1 Optical processes

Incident light can interact with the material in several ways depending on the energy of light and the properties of the material. The crucial processes for this study are absorption and different luminescence mechanisms such as up- and downconversion.

In absorption, if an incident light has a photon with energy corresponding to a transition of an electron, the photon gets absorbed and excites the electron to a higher energy

level. The energy and the wavelength of the photon are connected according to following equation

$$E = \frac{hc}{\lambda}, \tag{1}$$

where *E* is the energy of the photon, *h* is the Planck constant, *c* is the speed of light and λ is the wavelength of the photon.

Thus, absorption can also be considered as a function of wavelength. A schematic absorption process is depicted in Figure 3a.

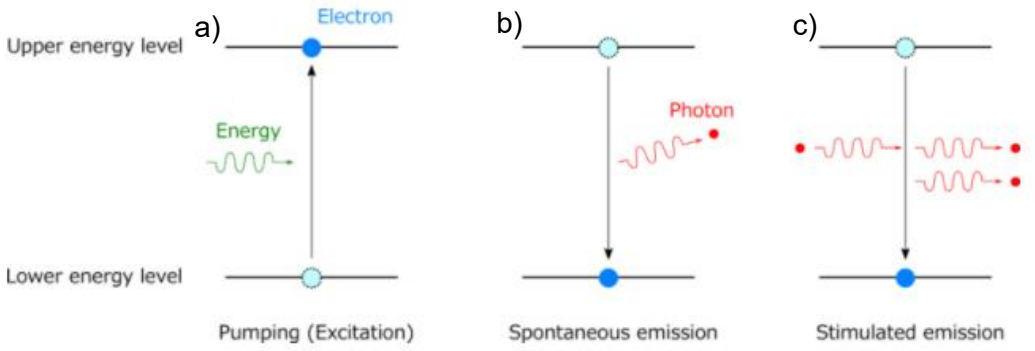

Figure 3: Schematic showing absorption of a photon followed by spontaneous and stimulated emissions. Modified from (FiberLabs Inc. n.d.)

When an excited electron falls back to its ground stage, the energy is released as a photon and the process is **spontaneous emission (Figure 3b) or downconversion**. In **stimulated emission (Figure 3c),** a passing photon forces an excited electron to fall and emit a photon that has the same phase and direction as the passing photon. Stimulated emission is used to amplify the signal, for example in optical fibers.

Upconversion (UC) process is a process, where at least two long wavelength photons are absorbed, but then only one photon with a shorter wavelength (or higher energy) is emitted. The three main upconversion mechanisms are presented in Figure 4.

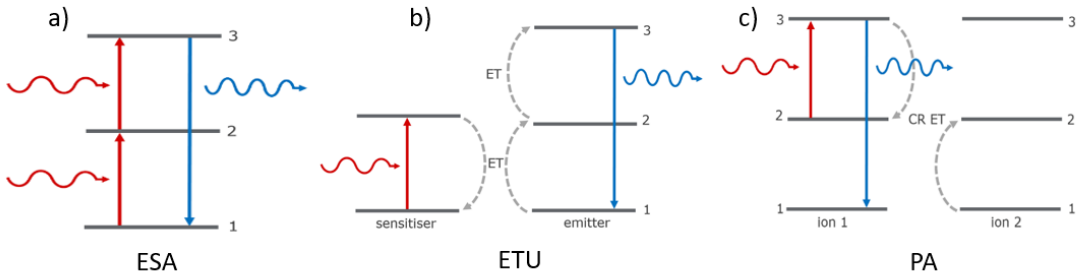

Figure 4: Main upconversion mechanisms of RE ions: Excited State Absorption, Energy Transfer Upconversion and Photon Avalanche. Modified from (Edinburgh Instruments 2018)

- **In Excited State Absorption (ESA),** first, a photon gets absorbed, and before an electron falls back to the ground stage, it absorbs another photon and jumps to higher stage. From the higher stage, the electron falls back to the ground stage. (Edinburgh Instruments 2018)
- **In Energy Transfer Upconversion (ETU),** the first ion absorbs a photon, and the electron jumps into the excitation stage, which is followed by energy transfer (ET) between two ions, and the second ion gets excited into a higher energy stage. (Edinburgh Instruments 2018)
- **In Photon Avalanche (PA),** an excited ion absorbs a photon, and an electron is excited to a higher energy level. Then cross relaxation energy transfer occurs; the energy of the excited electron is transferred to an ion in the neighbourhood. The first ion falls back to its first excitation state, and the ion neighbourhood is promoted to the excitation state. After the PA process, both ions can get excited with ESA or they can fall back to their ground stages. (Edinburgh Instruments 2018)

2.2.2 Er^{3+}-doped tellurite glasses

Erbium, yttrium, and ytterbium are the most common RE ion dopant. An external light pump can be used to excite electrons in an Er^{3+} ion, which absorbs light at certain wavelengths based on the electron transitions of the ion. In Figure 5, characteristic absorption spectrum and the corresponding electron transitions from the ground state to the different excited states are shown.

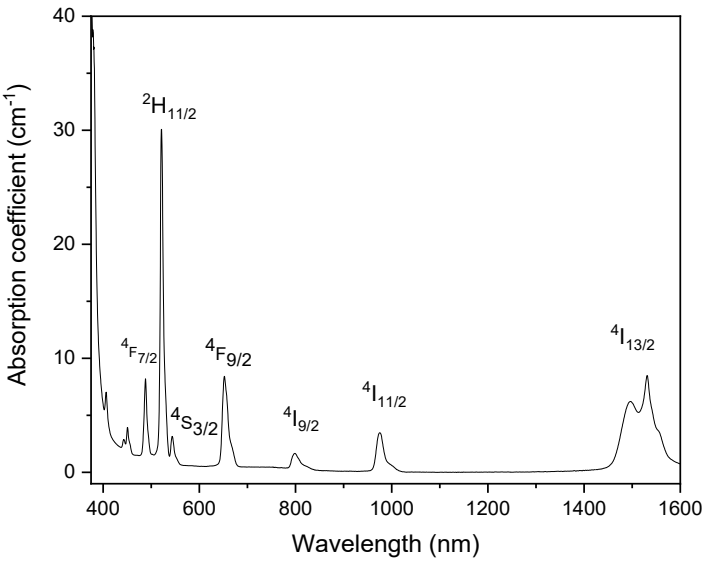

Figure 5: Schematic absorption spectrum of an Er^{3+}-doped glass and corresponding electron transitions from ground state $^4I_{15/2}$.

Energy levels of an Er^{3+} ion are illustrated in Figure 6, which shows ground state absorption (GSA), when an ion is excited with a 980 nm laser, possible UC processes; ESA and ETU, and obtained emission wavelengths.

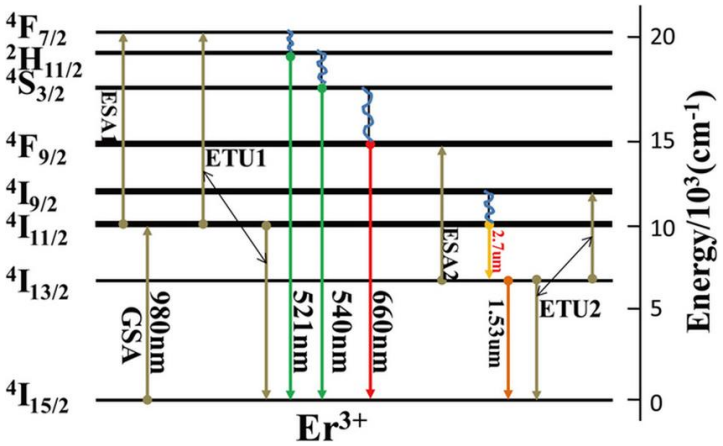

Figure 6: Schematic energy level diagram of Er^{3+}. (Y. Jiang 2016)

The 980 nm laser excites an electron from the ground state to the $^4I_{11/2}$ level. After that upconversion (UC) or downconversion (DC) process can occur.

- **In UC process,** the excited electron can absorb a second photon and jump to higher energy level. The de-excitation leads to emission of green and red lights.
- **In DC process,** a radiative emission from $^4I_{11/2}$ to $^4I_{13/2}$ leads emission at 2.7 µm, which is a very interesting wavelength for medical and spectroscopic applications (Y. Jiang 2016). The transition from the level $^4I_{13/2}$ to the ground stage $^4I_{15/2}$ results in an emission at 1.5 µm, which is an important wavelength used in telecommunication (J. Qi 2013).

A major advantage of using Er^{3+} ions is that all those transitions can be obtained by pumping the ion optically. On one hand, the efficient emission is hard to reach with low Er^{3+} ions concentration only. Hence, coupling Er^{3+} ions with, for example, other RE ions is an interesting area to study. (Z.A.S. Mahraz 2015) (M. S. M.R. Dousti 2013) On the other hand, the luminescence properties can be quenched by high Er^{3+} ion concentration. Indeed, a too large number of RE ions leads to ion clustering, and therefore, to concentration quenching, as well as a loss of excitation. Thus, it is crucial to determine the optimal concentration of RE ions to incorporate into a glass to optimize its spectroscopic properties. (D. Pugliese 2016) (M. S. M.R. Dousti 2013)

Tellurite glasses doped with Er^{3+} ions have attracted interest due to their good properties. For example, tellurite glass provides a lower phonon energy environment than other oxide glasses, which can enhance the quantum efficiency of the excited states of Er^{3+} ions (X. Shen 2020).

2.3 Silver in tellurite glasses

Recently, metallic nanoparticles (NP) have got a great deal of interest due to their possibility to enhance the luminescence properties of RE doped glasses.

2.3.1. Surface plasmon resonance

In theory, metallic NPs can improve luminescence efficiency through two different mechanism: either by energy transfer (ET) from metallic NP to the excited state of RE ion or by local field enhancement (LFE). Both processes rely on the surface plasmon resonance (SPR) of metallic nanoparticles. (D. da Silva 2007) However, studies have shown that energy transfer is negligible compared to enhancement caused by LFE (Z.A.S. Mahraz 2015).

Surface plasmon resonance can be illustrated as the oscillation of free electrons at the surface of metallic NP interacting with light as illustrated in the schematic picture in Figure 7.

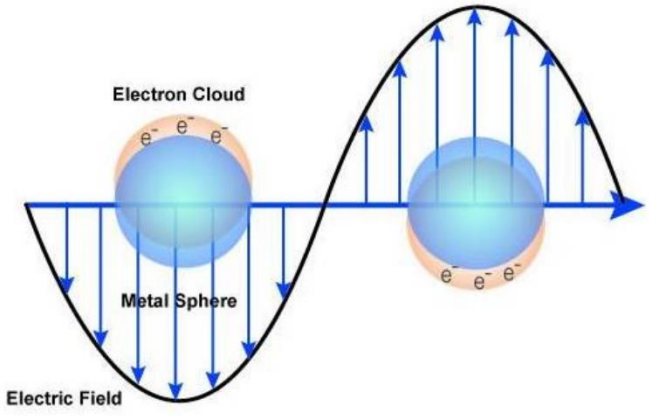

Figure 7: Cartoon of the oscillation.

Due to SPR, the local field around metallic nanoparticle is improved. If a RE ion is located close to the nanoparticle, the photonic density is increased around the RE ion. As a result, more photons can be absorbed by the RE ion leading to higher excited state population increasing the probability of transition from the excited state to the ground state, and therefore emission efficiency is enhanced. (J. Qi 2013) (H. E. H. Fares 2014)

Because surface plasmon resonance relies on the surface electrons, the effect of SPR is highly related to the type, shape, and size of the metallic nanoparticle. Furthermore, the enhancement efficiency also depends on the excitation wavelength: the SPR intensity is strengthened when its wavelength is close to the incident beam wavelength. (Z. A. S. Mahraz 2013) (D. da Silva 2007)

2.3.2 Growth of silver nanoparticles in glasses

Silver nanoparticles have received a large amount of attention among all metallic nanoparticles due to their noteworthy properties. Silver NPs have the surface plasmon resonance in the visible range, and the SPR band of silver NPs is sharper and stronger than, for example, the SPR band of gold or copper NPs. (H. E. H. Fares 2014) (Z.A.S. Mahraz 2015)

Silver nanoparticles can be grown in glass in a few different ways:

- **the ion-exchange method**, in which the glass is immersed into a mixture containing metal ions and ion implantation, in which implantation systems is used to add metal ions into the glass and the nucleation is obtained using a high ion-fluence implantation (A. Simo 2012).
- **the melt-quench method** which was used in this study. Here, silver oxide is added to the glass during the glass preparation so that silver is first in an ionic form. Silver nanoparticles nucleate and grow during a heat-treatment at temperature slightly higher than the glass transition temperature (T_g). At that temperature, the viscosity of the glass allows the silver ions to rearrange together into nanoparticles. By changing the heat-treatment duration and temperature, it is possible to control the growth of the Ag nanoparticles. (X. Shen 2020)

- **the sol-gel method,** in which metal ions are placed first in sol and the nucleation is achieved in heat-treatment (M. Epifani 2000).

2.3.3 Silver in Er^{3+} doped tellurite glasses

Nowadays, glasses doped with silver NPs and Er^{3+} ions are acknowledged as pioneers and leaders in terms of materials for fiber amplifiers and solid-state IR lasers (B.N. Swetha 2021). A schematic energy level diagram of Er^{3+} ion and silver NP is presented in Figure 8 when excitation is 980 nm.

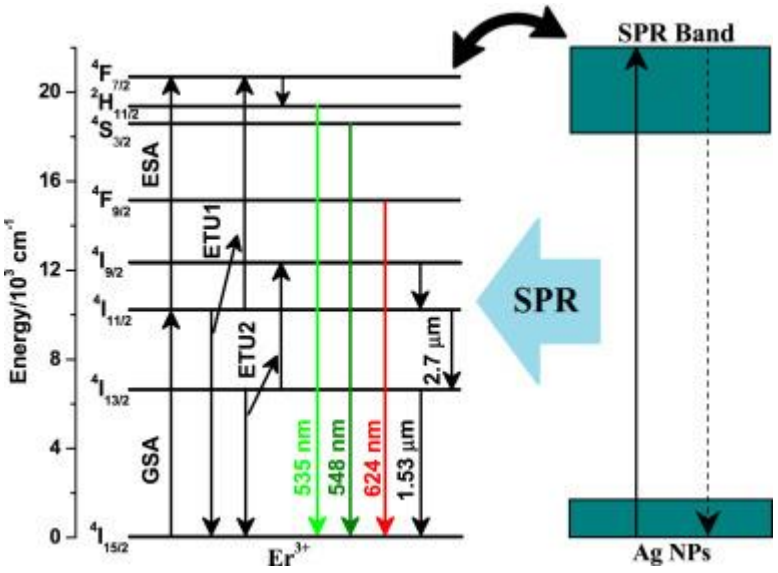

Figure 8: Schematic energy level diagram of Er^{3+} ion and silver NP. (B.N. Swetha 2021). The figure shows the SPR band, energy transfer between Er^{3+} ion and silver NP, the ground state absorption (GSA), excited state absorption (ESA), possible energy transfer upconversion (ETU1 and ETU2), and radiative emissions in different wavelengths.

The energy of 980 nm excitation is absorbed by the Er^{3+} ion, and it promotes an electron to jump from the ground state level to the $^4I_{11/2}$ level. Afterwards, the electron can absorb further and get excited to the $^4F_{7/2}$ level (ESA), or non-radiative relaxation can occur, and the electron falls to the $^4I_{13/2}$ level.

The enhancement of the emissions at 1.5 µm, at 2.7 µm and/or in UC processes when using Ag nanoparticles is due to SPR which increases the photonic density in the level $^4I_{11/2}$. (B.N. Swetha 2021) (J. Qi 2013) However, it should be mentioned that too large amount of silver NPs leads to emission quenching effect because of re-energy transfer from the excited state of Er^{3+} ion to the plasmon band of silver NP. (M. R. Dousti 2016) (B.N. Swetha 2021)

There are few studies focusing on the forming of silver nanoparticles in tellurite glasses. For example, H. Fares et. al studied the impact of heat-treatment on the spectroscopic properties of Er^{3+} doped tellurite glass with the composition $68.5TeO_2$-20BaO-$10Nb_2O_5$-

$1Er_2O_3$-$0.5AgNO_3$ (mol%) (H. E. H. Fares 2014). They demonstrated that a heat-treatment at slightly above T_g for at least 10 h leads to the formation of small Ag nanoparticles and so to an enhancement of the photoluminescence intensity associated with an increase in the lifetime of the $^4I_{13/2}$ level. This improvement was associated to the local electric field from the Ag nanoparticles and also to the energy transfer from silver to Er^{3+} ions. Similar results were reported by Qi et al (Y. Qi 2014) in glasses with the composition (77.5-x) TeO_2–20ZnO–$0.5Er_2O_3$–$2Yb_2O_3$–$xAgNO_3$ and by Mahraz et al (Z.A.S. Mahraz 2015) (Z. A. S. Mahraz 2013) in glasses with the composition (60-x)TeO_2 - $30B_2O_3$-10ZnO-$0.5Er_2O_3$- xAgCl (mol%). The intensity of the emission at 1.5 µm was found to increase by 62 % when heat treating the glass prepared with 0.5 mol% of $AgNO_3$ at around T_g for 24 hours (Y. Qi 2014). One should mention that an increase in the thermal stability of the glass was also observed when adding Ag in the tellurite network. Despite the promising results on adding Ag_2O on the spectroscopic properties of Er^{3+} ions in tellurite glasses, not so many studies have been focused on tellurite glasses embedded with Er^{3+}-ions containing Ag_2O.

Therefore, the goal of this study is to check if it is possible to grow silver nanoparticles in Er^{3+} doped tellurite glass in the TeO_2-ZnO-Bi_2O_3 system to enhance the spectroscopic properties of the glass. In this glass system, tellurite oxide is the glass former and forms the glass network, zinc oxide acts as an intermediate and/or glass modifier, and bismuth oxide is a glass intermediate. Zinc and bismuth oxides substitute glass former and modify the properties of the glass. Based on the previous studies (J.Massera 2010), this glass system was found to exhibit bulk crystallization during heat-treatment and therefore is a good candidate for the preparation of glass-ceramic.

3. EXPERIMENTAL PART

3.1 Glass preparation

Glasses with the composition (100-x-y) ($70TeO_2$-$20ZnO$-$10Bi_2O_3$)-xAg_2O-yEr_2O_3 with x = 0, 0.5 ,1, 2 and 4 and y = 0 and 2.5 mol% were prepared using the melting quenching technique. The raw materials were TeO_2 (Alfa Aesar, ≥ 99 %), ZnO (Aldrich, 99.99 %), Bi_2O_3 (Aldrich, 99.9 %), Er_2O_3 (Aldrich, ≥ 99.99 %) and Ag_2SO_4 (Sigma-Aldrich, ≥ 99,5 %). Different compositions and their respective names are shown in Table 1.

Table 1: The compositions of the investigated glasses. Erbium-free glasses are made just for as reference samples. They are in italics in the Table 1 and labelled Er0Ag0, Er0Ag1 whereas the Er^{3+} doped glasses are labelled Agx with x=0, 0.5, 1, 2, 4.

Name	TeO_2 (mol%)	ZnO (mol%)	Bi_2O_3 (mol%)	Er_2O_3 (mol%)	Ag_2SO_4 (mol%)
Ag0	68.3	19.5	9.8	2.5	0
Er0Ag0	70	20	10	0	0
Ag0.5	67.9	19.4	9.7	2.5	0.5
Ag1	67.6	19.3	9.7	2.5	1
Er0Ag1	69.3	19.8	9.9	0	1
Ag2	66.9	19.1	9.6	2.5	2
Ag4	65.5	18.7	9.4	2.5	4

The chemicals were weighted, grinded and then homogeneously mixed in a mortar. The 17 g batches were placed into a quartz crucible and then melted in a furnace. Er-free glasses were melted at 750 °C and glasses doped with Er^{3+} ions at 775 °C for 40 minutes. To obtain a homogenous mixture, the melts were carefully stirred after 20 minutes at the melting temperature. The melted glasses were quenched by pouring them rapidly onto a copper plate and then annealed for 6 hours at 200 °C to remove the residual stress from the quench. The glasses were slowly cooled down to room temperature. Finally, glasses were polished.

To grow silver nanoparticles and study the effect of heat-treatment duration, the glasses were heat-treated at 20 °C above their respective glass transition temperature (T_g) for 2, 5, and 17 hours with a heating rate of 10 °C/min.

3.2 Differential Scanning Calorimetry

To determine the thermal properties of the glasses, Differential Scanning Calorimetry (DSC) was used. An example of a thermogram and glass characteristic temperatures are shown in Figure 9.

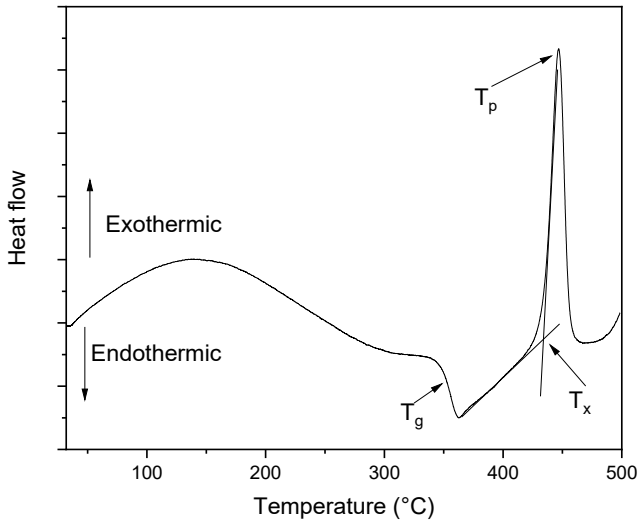

Figure 9: Thermogram of the Ag0 glass, taken as an example. The characteristic temperatures are pointed out.

The thermal properties can be described with the glass transition temperature (T_g), the onset of the crystallization peak (T_x) and the crystallization temperature (T_p).

At glass transition temperature, the glass begins to transform from solid to liquid. Transformation occurs in the glass transformation region and it is the matter of discontinuous change in the heat flow which can be seen in Figure 9. In this study, the T_g was determined as the inflection point of the first endothermic peak, and it was verified by taking the first minimum of the derivative of the thermogram. T_x was determined as an onset point of crystallization and T_p as a maximum of the exothermic peak.

During DSC measurements, an inert reference sample and the studied sample are heated under controlled conditions. Every thermal process including phase transitions, crystallization and glass transformation affect the sample while the reference sample follows the heating rate. The heat flow difference between the reference and the sample can be plotted as a function of temperature.

The thermograms were measured using a Netszch F1 instrument. A small amount of every sample was ground into rough powder which was heat treated from 40 to 500 °C with an accuracy of ± 3 °C using a 10 °C/min heating rate.

3.3 Density

The density of glass was determined by using a simple Archimedes' law which can be written as the following equation according to

$$F_b = V\rho_f g, \tag{2}$$

where F_b is the buoyant force, V is the volume of immersed piece, ρ_f is the density of the immersive fluid and g is the standard acceleration of freefall (lumencandela 2016). Equation 2 can be derived into a very usable form with help from Newtons first and second laws. A new equation can be expressed as

$$\rho = \frac{\rho_l m_a}{m_a - m_l}, \tag{3}$$

where ρ is the density of studied sample, ρ_l is the density of the immersion liquid, m_a is the mass of the sample in air and m_l is the mass of the immersed sample.

The density of glasses was determined using ethanol as an immersion liquid. First, the glasses were weighted in air with an electric scale and then weighted again into ethanol. The accuracy of the measurements is ± 0.02 g/cm^3.

3.4 XRD

A crystalline structure of glass can be determined by using X-Ray Diffraction (XRD). Crystal has an organized structure, whereas ordinary glass is totally amorphous. In crystallized samples, atoms form atom planes, which are parallel to each other. Depending on the distance between the planes, diffraction of X-Rays can create either constructive or destructive interferences.

XRD measurements are based on constructive interferences which happen only in a certain circumstance. If conditions fulfill Bragg's Law (Equation 4), constructive interference occurs, and peaks appear in the XRD pattern. (Barbara L Dutrow, X-ray Powder Diffraction 2020) Bragg's Law can be written as

$$n\lambda = 2dsin\theta, \tag{4}$$

where *n* is an integer, λ is the wavelength of the X-Ray, *d* is the distance between the planes and θ is the diffraction angle.

Schematic picture of X-Ray diffractometer (XRD) is illustrated in Figure 10.

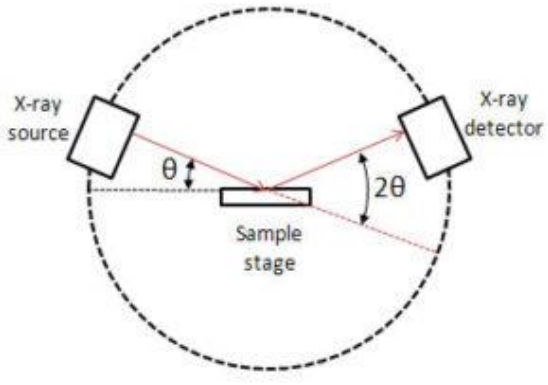

Figure 10: Schematic of XRD. (xrd.co n.d.)

In an X-Ray Diffractometer, the generated and collimated X-Rays reach the sample at an angle of θ. After the interactions with the sample, the diffracted X-Rays are collected by the detector. As can be seen in Figure 10, the detector is placed at an angle of 2θ to satisfy the Bragg's law (Equation 4). To examine every diffraction angle, the sample is scanned through a range of 2θ angles by moving the X-Ray tube and detector along a

circle. Therefore, the collected diffraction pattern spectrum is determined as a function of the incident angle. (Barbara L Dutrow, X-ray Powder Diffraction 2020)

Since every crystal has its own and unique structure, X-Ray diffractometer creates a unique diffraction pattern depending on the atoms in the crystals. As a result, the structure of the studied sample can be determined by comparing its diffraction pattern to a database.

The XRD measurement was done using Panalytical EMPYREAN multipurpose X-Ray Diffractometer. The X-Ray patterns were measured in bulk samples which were placed onto a sample holder.

3.5 Raman spectroscopy

To analyze the structure of the glass and, to be precise, the molecular units forming the network of the glasses, the Raman spectroscopy was used.

Raman spectroscopy is based on light scattering from the sample. Interactions between light and media during the scattering process can change the energy and therefore the wavelength of the scattered light. The light scattered at the same wavelength is called Rayleigh scattering, and it does not provide helpful information of the sample structure. However, if the wavelength changes during scattering process, the phenomenon is called Raman scattering, and Raman spectroscopy is based on it. (Edinburgh Instruments 2021)

Raman scattering is an inelastic photon scattering process, in which energy transfer between a molecule and a scattered photon occurs. In Stokes Raman scattering, the photon excites the molecule to a higher vibrational level and at same time loses part of its energy. In contrast, in anti-Stokes Raman scattering, the molecule relaxes into a lower vibration level and the photon gains the corresponding energy. (Edinburgh Instruments 2021) Rayleigh, Stokes, and anti-Stokes scattering events are depicted in Figure 11.

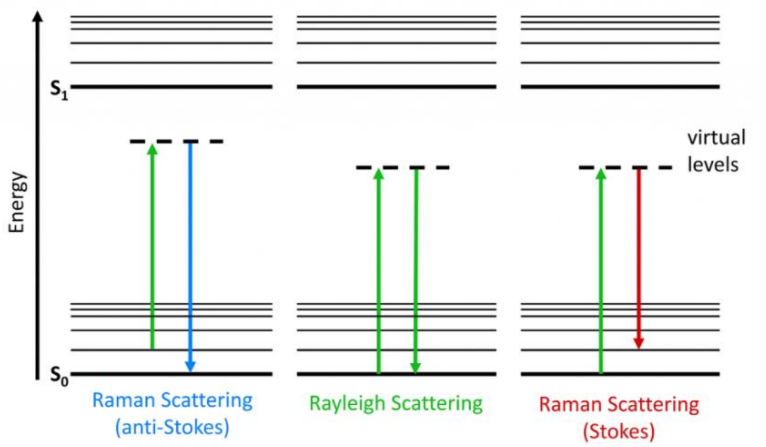

Figure 11: Energy transitions in Rayleigh and Raman scattering. (Edinburgh Instruments 2021)

In Raman spectroscopy, the studied sample is irradiated by a laser and only Raman scattered photons are collected by using filters, lens, and detector. A difference between the wavelength or the incident light and Raman scattered photons provides information of the vibrational energy modes and molecular bands of the studied sample.

The Raman spectra were measured on polished glasses and wavenumber in range from 200 to 1300 cm^{-1} with Renisher inVia™ Qontor. using 785 nm laser excitation.

3.6 Optical properties

If an incident light possesses photons with equivalent energy to a transition of an electron, then it is absorbed, and the electron jumps into a higher energy stage. In other words, a photon gives its energy to an electron and disappears. Therefore, the intensity of the light decreases. Due to the dependence between the photon energy and the wavelength, the absorption can also be described as a function of wavelength.

An optical instrument which measures the light intensity absorbed by a sample as a function of wavelength is called spectrometer. A schematic layout of spectrometer is depicted in Figure 12.

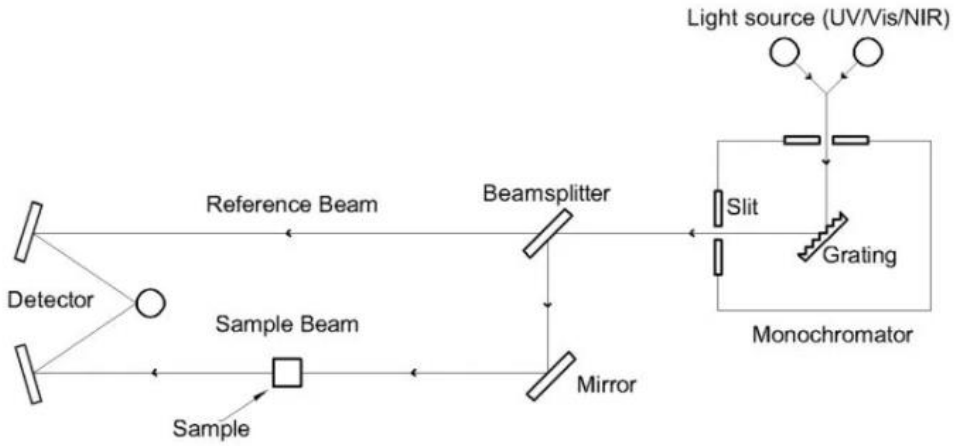

Figure 12: Schematic diagram of spectrometer. (Shelby 2005)

A spectrometer consists of a light source, a monochromator, a beam splitter, mirrors, and a detector. The monochromator includes a grating and a slit, and it selects a narrow wavelength range from the light source and makes it monochromatic. The beam splitter splits the beam into two parts: a Reference Beam and a Sample Beam. With mirrors, the Reference Beam is guided straight to the detector whereas the Sample Beam travels through the studied sample on its way to the detector. Finally, the detector collects the intensities of both beams.

The absorbance of the sample (*A*) is defined by the equation bellow:

$$A = \log\left(\frac{I}{I_0}\right), \tag{5}$$

where I is the intensity of Sample Beam and I_0 is the intensity of the Reference Beam.

From Beer Lambert law (Chemistry LibreTexts 2020),the intensity of the Sample Beam can be expressed as

$$I = I_0 e^{\alpha l}, \tag{6}$$

where α is the absorption coefficient and *l* the thickness of the sample.

Therefore, the absorption coefficient can be obtained using the equation:

$$\alpha = \frac{\ln(10)}{l} A. \tag{7}$$

The absorption cross-section illustrates how the system absorbs light per absorbing ion. The absorption cross-section can be calculated using the following equation:

$$\sigma_{abs} = \frac{\alpha}{N}, \tag{8}$$

where α is the absorption coefficient and *N* is RE-ion concentration (ions/cm^3).
The absorption cross-sections were determined with an accuracy of ± 10 %.

An UV-Vis-NIR -spectrophotometer (UV-3600 Plus, Shimadzu) was used to measure the absorption spectra using polished samples. The thicknesses of the polished samples were determined using a digital caliper and the accuracy of the measurement is ± 0.05 mm.

3.7 Emission spectra measurement

A spontaneous emission of light is called luminescence. It occurs when an exited electron falls back to its ground stage and energy is released as a photon. The emission spectra can be collected using a spectrofluorometer which is an optical instrument. The schematic of it is illustrated in Figure 13.

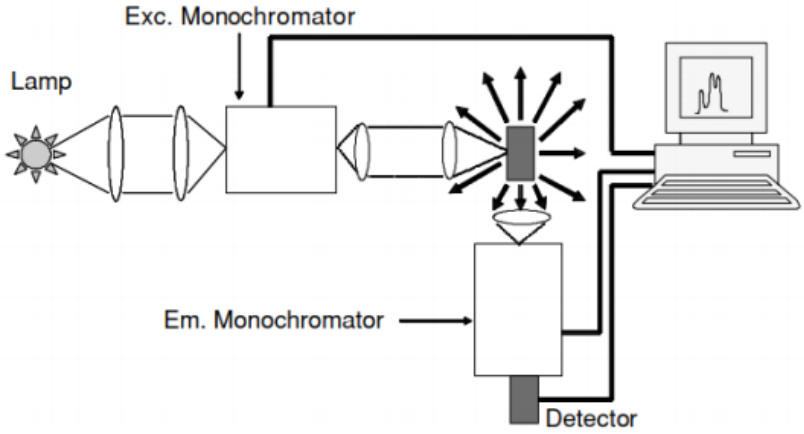

Figure 13: Schematic picture of a spectrofluorometer. (J.G. Solé 2005)

The spectrofluorometer setup consists of an excitation source which can be either a laser or a lamp, two monochromators, lenses, and a detector. First, electrons are excited with monochromatic light after which the emitted light is collected and focused by using lenses. The emitted light beam goes to the monochromator and then to the detector. The monochromator allows only a certain wavelength to pass through; thus, the detector measures an intensity of the emission at one wavelength at a time. An emission spectrum is plotted by scanning wavelength by wavelength over given range.

The emission spectra measurements were carried out by using a 976 nm single-mode fiber pigtailed laser diode (CM962UF76P10R, Oclaro), a Jobin Yvon iHR320 spectrometer, a Hamamatsu P4631-02 detector and a Thorlabs FEL 1500-filter. Before measurements, a small piece of every glass was crushed into a fine powder and placed in a sample holder. The emission spectra centered around 1.5 µm was measured using the range 1400-1700 nm and upconversion using the range 500-750 nm. To confirm the results, every measurement was repeated twice with two different samples. The difference between measurements should be below 10 % accuracy.

4. RESULTS AND DISCUSSION

The goal of this study was to prepare new Er^{3+}-doped tellurite glasses in the TeO_2-ZnO-Bi_2O_3-Ag_2O system to check if Ag nanoparticles can be grown in the glass using heat to enhance the spectroscopic properties of the glasses. At first, glass preparation process was explained, then the impact of the Ag_2O addition on various glass properties was discussed and finally the effect of heat-treatment on the Ag nanoparticles formation in the newly developed glasses and also on the spectroscopic properties of the glass were studied.

4.1 Preparation of tellurite glass with silver NPs

The first task of this project was to prepare tellurite glasses with the Ag precursor ($AgSO_4$). Due to the presence of Ag, the investigated glasses could not be prepared in a Pt crucible which is typically used when melting tellurite glasses as silver can actually react with platinum. Thus, the batches were melted in quartz crucible in this study.

The Ag free glass was successfully prepared in Pt crucible using a melting temperature of 850 °C for 20 minutes. However, when similar glass was prepared in quartz using the same melting process (temperature and duration of the melting), the Ag free glass crystallized during the quenching as depicted in Figure 14.

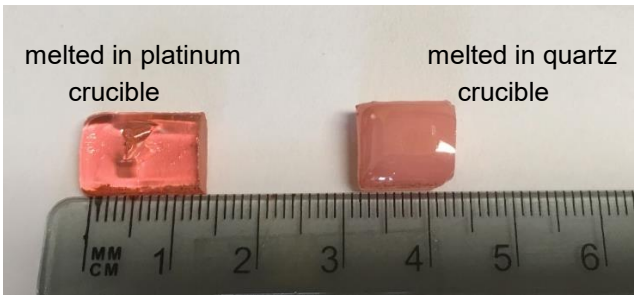

Figure 14: A photograph of tellurite glasses melted in platinum and quartz crucibles.

Even though quartz crucible is considered as an inert crucible, diffusion of Si from the crucible to the melt is suspected to occur during the melting. It is the presence of Si which is thought to induce crystallization during quenching.

If this hypothesis is right, the Si contamination could be attenuated by reducing the melting temperature and also the duration of the melting. Thus, glasses were prepared using different melting parameters. The melting trials can be found in Table 2.

Table 2: Used melting parameters and remarks

Melting temperature (°C)	Melting time (minutes)	Observations
850	20	Crystalized
700	120	Didn't melt properly, regardless long melting time Melting temperature was too low
750	20	Glass melt wasn't homogenous, obtained glass had crystals/ nonho-mogeneous parts
750	40	Glass melt wasn't homogenous, obtained glass had crystals/ nonho-mogeneous parts
750	60	With small batch these melting conditions suited but with larger batch glass didn't melt properly Melting temperature was still too low
775	40	Obtained glass was homogeneous and transparent

A decrease in the melting temperature requires an increase in the melting time to obtain a homogeneous mixture as a lower temperature demands more time to melt the raw chemicals. On the other hand, a possible Si diffusion from the crucible to the glass can occur when the melting duration is too long. Therefore, a compromise to find the best melting conditions was crucial. Per our trials, the glasses in this study were prepared using a melting temperature of 775 °C and a melting duration of 40 minutes.

4.2 Characterization of the investigated glasses

Glasses with the composition (100-x-y) ($70TeO_2$-$20ZnO$-$10Bi_2O_3$)-xAg_2O-yEr_2O_3 with x = 0, 0.5,1, 2 and 4 and y = 0 and 2.5 mol% were fabricated using the melting quenching technique and quartz crucible.

The densities and thermal properties of as-prepared glasses are shown in Table 3.

Table 3: Thermal properties and densities of the investigated glasses.

Glass	T_g ± 3 (°C)	T_x ± 3 (°C)	T_p ± 3 (°C)	$\Delta T=T_x-T_g$ ± 6(°C)	ρ ± 0.02 (g/cm^3)
Er2.5Ag0	353	434	446	81	6.20
Er2.5Ag0,5	352	436	448	84	6.19
Er2.5Ag1	349	434	448	85	6.18
Er2.5Ag2	342	438	455	96	6.17
Er2.5Ag4	332	421	473	89	6.15
Undoped glasses					
Er0Ag0	333	467	499	134	6.09
Er0Ag1	326	386	504	60	6.10

The density decreases when the Ag_2O concentration increases. It is due to the molar mass of Ag_2O, which is lighter than the molar mass of TeO_2 and Bi_2O_3. Therefore, an increase in silver oxide concentration decreases the amount of heavier oxides in the glass. Also shown in Table 3 is the density of undoped glasses. As for Ag, the addition of Er^{3+} ions in the glass increases the density due to the heavy Er^{3+} ions.

The thermal properties of the glasses were determined using data from DSC, and thermograms are presented in Figure 15.

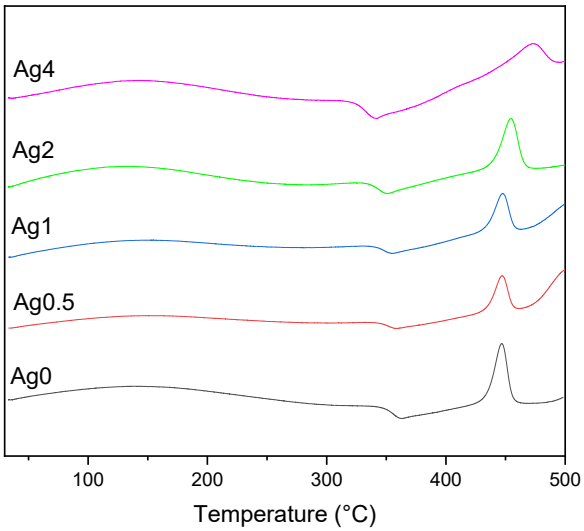

Figure 15: DSC curves of the glasses.

When the Ag_2O concentration increases, T_g decreases and T_x and T_p increase. This is probably the result of the silver that enters in the tellurite glass leading to changes in the glass network (Y. Qi 2014). The ΔT (T_x - T_g) is a rough estimator of the thermal stability of the glass against crystallization. Thermal stability is an important parameter to know, especially if the goal is to draw a fiber. Because of fiber drawing is a reheating process, crystallization during the drawing can occur if the glass is not thermally stable leading to an increment in the scattering losses of the fiber. The ΔT should be at least 100 °C so the glass can be considered stable against crystallization. (Y. Qi 2014) As the Ag_2O concentration increases, ΔT increases up to almost 100 °C indicating that these glasses can be considered as thermally stable against crystallization. As shown in Table 3, the addition of Er^{3+} ions has also an impact on the thermal properties: it increases T_g and T_x but decreases T_p.

In Figure 16, the Raman spectra of the as-prepared glasses are shown. Every spectrum is normalized according to the band at 660 cm^{-1}. Therefore, the changes in the Raman spectra due to the addition of Ag_2O are relative to this band.

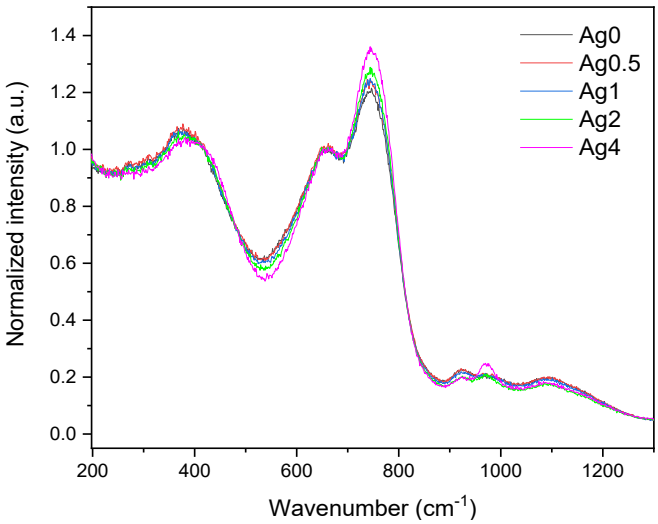

Figure 16: Normalized Raman-spectra.

The spectra exhibit bands at ~370, 660, 770, ~920, ~975 and 1100 cm^{-1}. The band around 370 cm^{-1} can belong to Zn-O according to (R.J. Amjad 2013) and also to Bi-O-Bi vibrations (J. Massera 2010), the band at 660 cm^{-1} is related to stretching of Te-O bond in TeO_4 units, and band at 770 cm^{-1} belongs to more disordered TeO_3 and/or TeO_{3+1} units, in which one Te-O bond is lengthened (T. Sekiya 1992). The intensity of the band at 770 cm^{-1} increases compared to that of the band at 660 cm^{-1}, when the Ag_2O concentration increases indicating that the TeO_4 network is disrupted with an increase in the TeO_3 and/or TeO_{3+1} units at the expense of TeO_4 units (T. Sekiya 1992). The Raman spectra exhibit bands between 900 and 1200 cm^{-1}, the attribution of which is still under investigation.

The absorption spectra of as-prepared glasses can be seen in Figure 17.

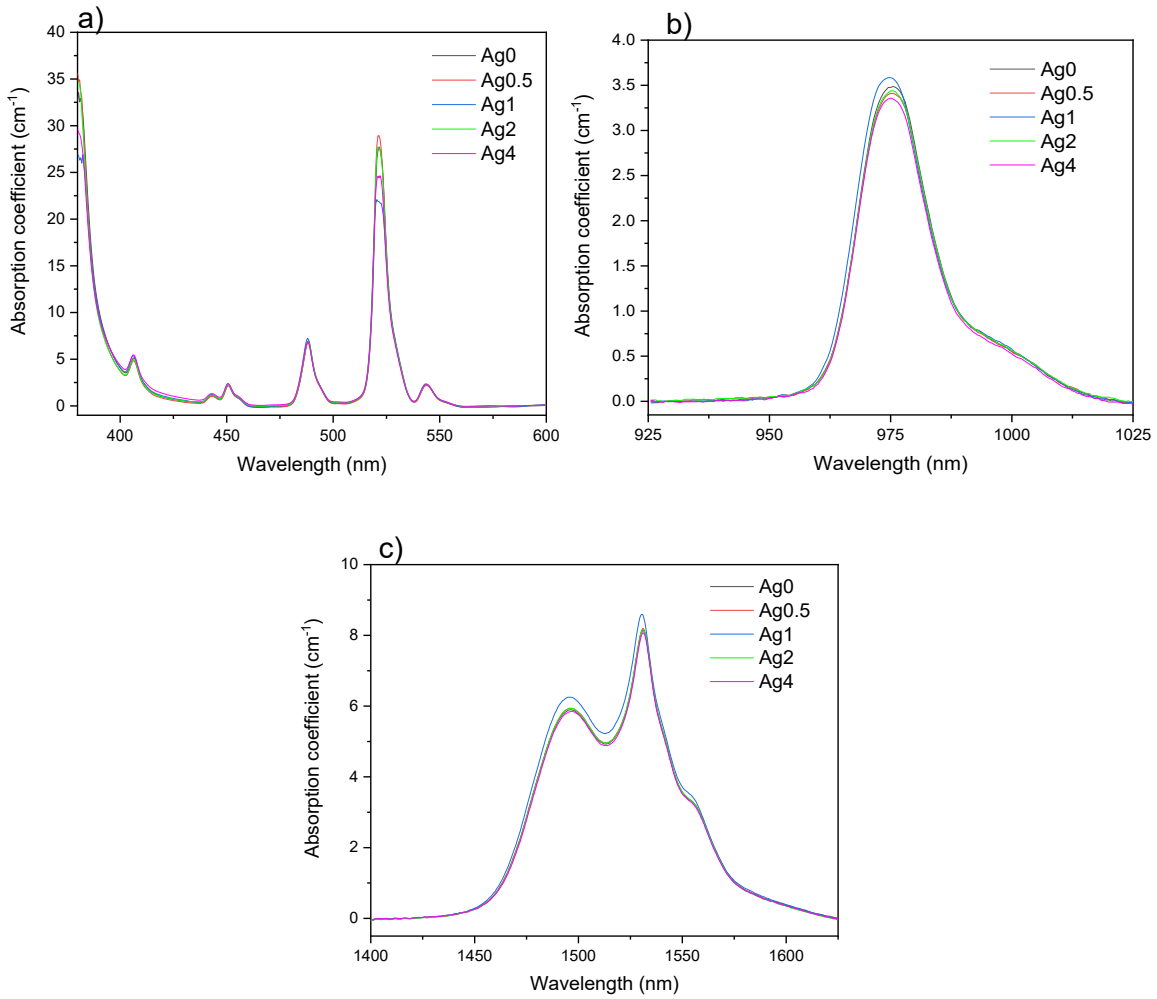

Figure 17: Absorption spectra of glasses (a), absorption band at 980 nm (b), absorption band at 1530 nm (c).

The spectra exhibit absorption bands which are related to the electron transitions of Er^{3+} ions from the ground state $^4I_{15/2}$ to the excited state. For example, the band at around 980 nm can be attributed to the transition from the ground state to the $^4I_{11/2}$ level. An increase of silver oxide concentration leads to neither a notable shift of the band gap nor a new absorption band around 450 nm, which could be related to the silver surface plasmon resonance (SPR) band. Thus, silver is expected to be in the glass in ion form.

Figure 17b and c show the bands which were used to determine the absorption coefficients at 975 and 1531 nm. From the absorption coefficients and Equation 8, the absorption cross-sections were calculated, and results can be seen in Table 4.

Table 4: The absorption coefficients (α_{abs}), Er^{3+} ion concentrations and absorption cross-sections (σ_{abs}).

	α_{abs} at 975 nm (cm^{-1})	α_{abs} at 1531 nm (cm^{-1})	$Er^{3+}(10^{21})$ ($ions/cm^3$) ± 5 %	σ_{abs} at 975 nm (10^{-21}) (cm^2) ± 10 %	σ_{abs} at 1531 nm (10^{-21}) (cm^2) ± 10 %
Ag0	3.48	8.42	1.04	3.36	8.13
Ag0.5	3.41	8.33	1.04	3.30	8.04
Ag1	3.58	8.58	1.03	3.48	8.32
Ag2	3.44	8.17	1.03	3.35	7.97
Ag4	3.36	8.08	1.01	3.31	7.96

The differences between absorption cross-sections are within 10 % accuracy indicating that an increase in the Ag_2O concentration has negligible influence on the absorption cross-sections at 975 and 1531 nm and so on the site of Er^{3+} ions even though the progressive addition of Ag_2O modifies the structure of the glass.

The emission spectra of the upconversion process are shown in Figure 18. The excitation was 976 nm. Figure 18a shows the normalized upconversion spectra according to the intensity at 669 nm.

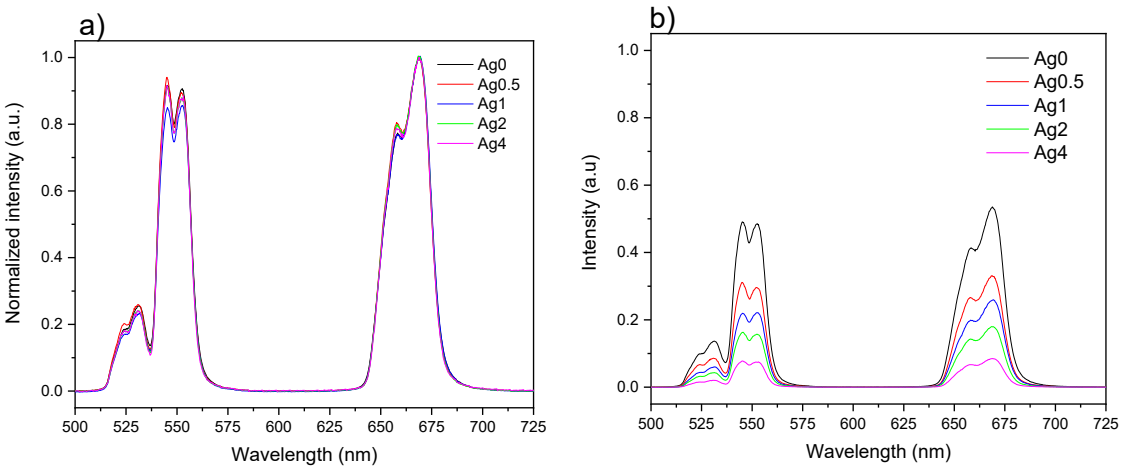

Figure 18: Normalized upconversion spectrum of the investigated glasses (a) and intensity of the emission at 550 and 660 nm as a function of Ag_2O content (b).

The spectra exhibit the typical green and red emission bands of Er^{3+} ions in tellurite glasses. The band around 550 nm corresponds to the transition from the $^4S_{3/2}$ level to the ground state and the band around 660 nm is attributed to the transition from the $^4F_{9/2}$ level to the ground state. The broad bands confirm that the Er^{3+} ions are located in amorphous site. One can notice that the glasses, independently of their composition, exhibit similar emission band confirming that the Er^{3+} sites are similar in all the glasses. Silver is not assumed to enter in the coordination shell of Er^{3+}. However, as depicted in Figure 18b, an increase in Ag_2O concentration leads to a decrease in the intensity of the green

and red emission. It is possible that because of the depolymerization of the tellurite network, the distances between the Er^{3+} ions increasing reducing then the upconversion process.

The emission spectra around 1.5 μm are presented in Figure 19. The excitation source was 976 nm laser diode, and the spectra have been normalised according to the intensity at 1532 nm.

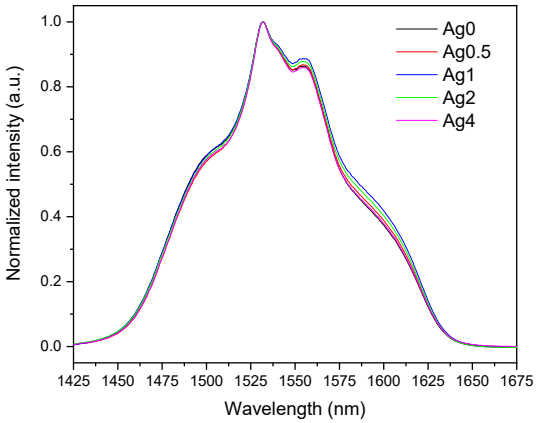

Figure 19: Normalized Emission spectrum of the investigated glasses.

A typical emission band for Er^{3+} ions in a tellurite glass environment can be seen in Figure 19. This band belongs to the electronic transition from the $^4I_{13/2}$ level to the ground state. It is clearly shown that an increase in the silver oxide concentration has a negligible effect on the shape of the emission at 1.5 μm while no changes in the intensity of the emission at 1.5 μm were noticed confirming that the Er^{3+} sites are Ag free.

4.3 Influence of heat-treatment on the formation of Ag NPs

According to (H. E. H. Fares 2014) a heat-treatment near the glass transition temperature can lead to the precipitation of Ag nanoparticles in glasses. Therefore, the glasses were heat-treated at T_g + 20 °C for 2, 5, and 17 hours. After heat-treatment, the light pink color of the glasses transformed into first, a more orangish color glass, and finally, after 17 hours at heat-treatment, glasses were not transparent anymore, as can be seen in Figure 20.

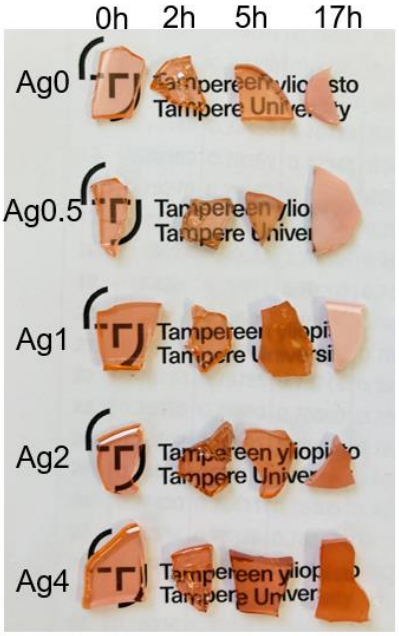

Figure 20: A photograph of heat-treated glasses.

In Figure 20, it is easy to notice that a major change in the glass transparency occurs between 5 and 17 hours of heat-treatment. Additionally, the opacity level of the glasses depends on the Ag_2O content: an increase in the Ag_2O content leads to less opaque glasses. This is in agreement with the thermal properties of the glasses; indeed, an increase in the Ag_2O content increases ΔT confirming that the highly Ag concentrated glasses are the least prone to crystallization than the Ag0 glass, for example.

The change in transparency can be related to the crystallization of the glasses which was confirmed by using XRD. The XRD pattern of the glasses are presented Figure 21.

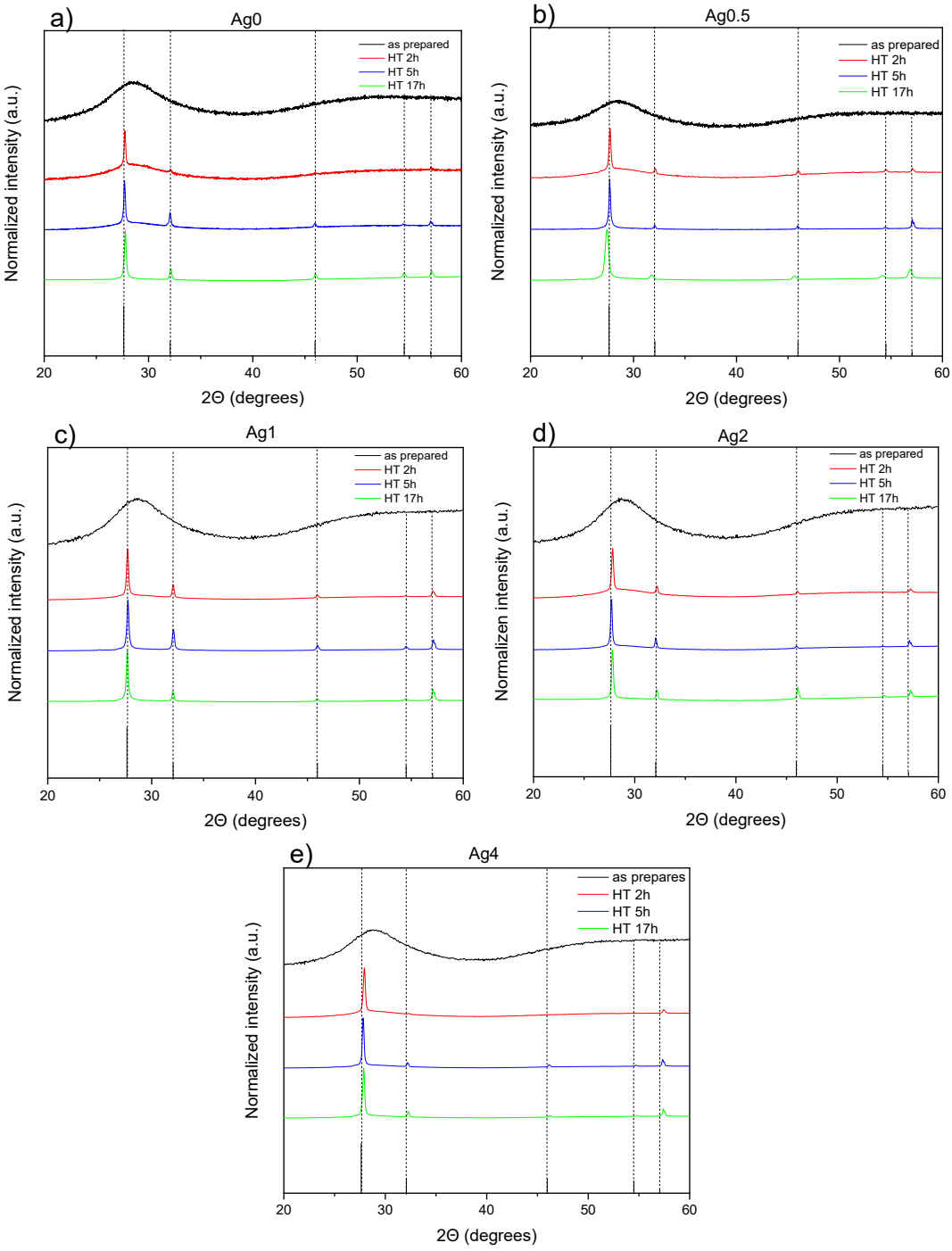

Figure 21: XRD patterns of heat-treated glasses compared to the pattern of Bi_4TeO_8 crystals.

All the as-prepared glasses exhibit broad band confirming their amorphous structure. Sharp peaks occur in the XRD pattern of the glasses after heat-treatment verifying that crystallization appeared during heat treatment although the temperature was T_g + 20 °C. All XRD patterns of the heat-treated glasses exhibit peaks almost at the same angles, and those peaks can belong to the Bi_4TeO_8 crystal (ICDD 00-024-0157). The intensity of the peaks related to this crystal increases as compared to the intensity of the broad band with an increase in the duration of the heat treatment indicating the growth of this crystal with an increase in the heat treatment duration.

The XRD pattern clearly shows that the glasses after heat treatment for 2 to 5 hours are transparent glass-ceramics. One can also notice that a longer heat-treatment duration shifts peaks to the left; according to Bragg's Law (Equation 4), a shift to the left indicates that the distance between atom planes increases, and as an inverse, shift to right indicates a decrease of the distance between atom planes.

One should point out that a peak with small intensity can be seen at ~38.18° (Figure 22).

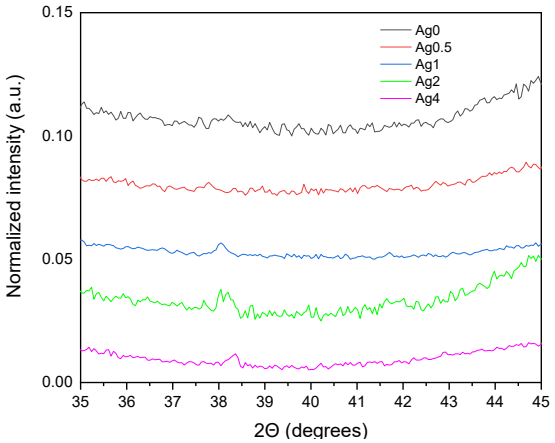

Figure 22: Zoomed XRD pattern of the glasses heat-treated for 17 hours at T_g+20 °C.

According to (K. Shameli 2012) this peak could be attributed to Ag nanoparticles. Due to the small intensity of this peak, the silver nanoparticles are expected to be small and in low number in the glasses.

The absorption spectra of heat-treated samples are presented in Figure 23. Since the samples heat-treated for 17 hours and sample Ag1 heat-treated for 5 hours are opaque, they scatter the light, and absorption cannot be determined for them in the same way as the transparent samples, so they are not presented in Figure 23.

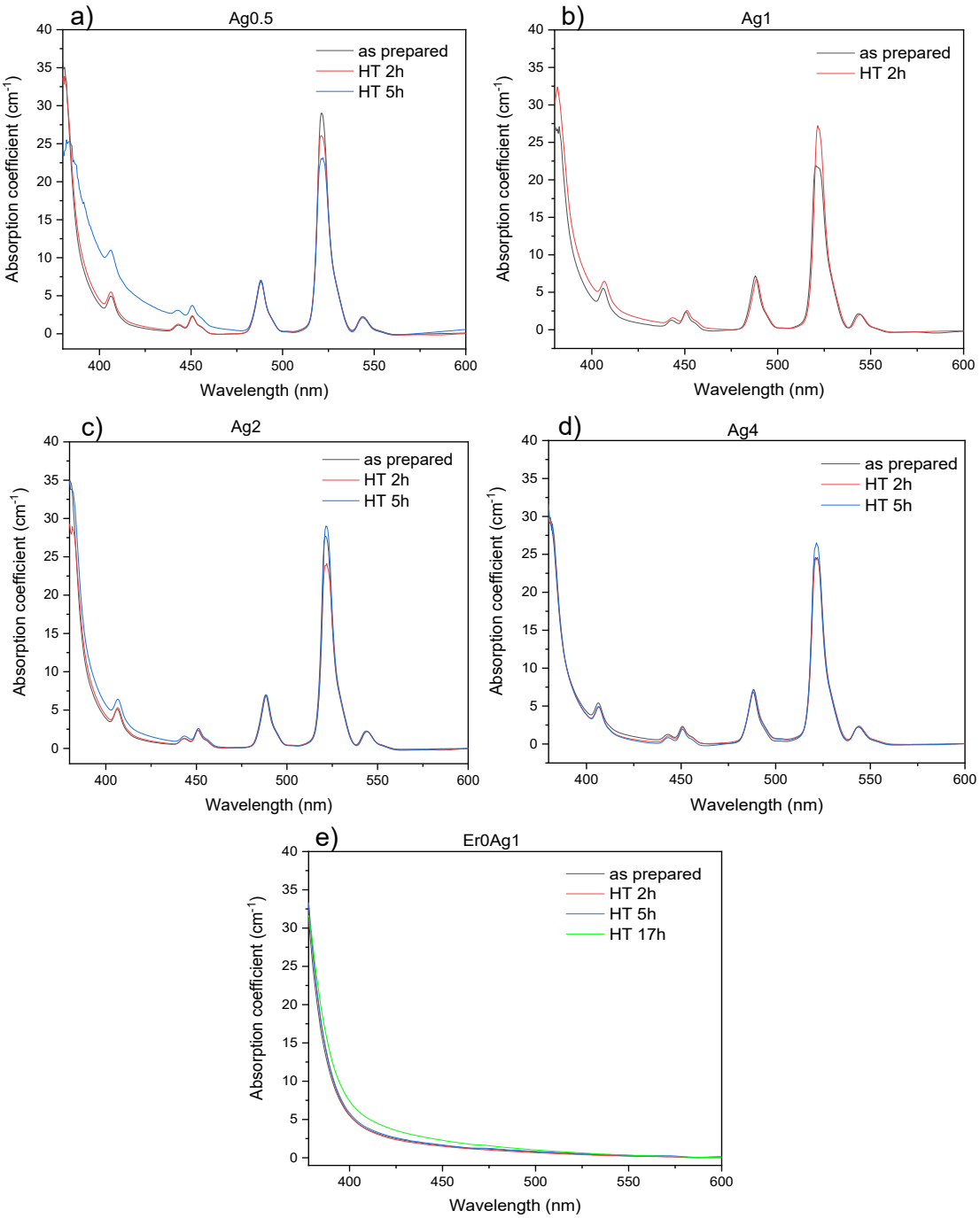

Figure 23: Absorption bands of the glasses after heat-treatment.

No noticeable changes in the absorption spectra were seen after heat-treatment indicating a weak surface plasmon resonance (SPR) band in agreement with the analysis of the XRD pattern. According to some studies (M. S. M.R. Dousti 2013), weak SPR band can overlap with the absorption band of Er^{3+} ions and so cannot be observed from absorption spectra. However, no SPR absorption band can be observed after heat treatment in the absorption spectrum of Er free glass as depicted in Figure 23e confirming that the heat-treatment probably did not lead to the precipitation of Ag nanoparticles in large concentration. The absorption cross-sections of the glasses heat-treated for 2 and

5 hours were calculated. Within the accuracy of the measurements, neither the absorption coefficient nor the cross-section changes after heat-treatment, which implies the similar site of Er^{3+} ions prior to and after heat treatment.

The upconversion spectra of the glasses before and after heat-treatment are presented in Figure 24.

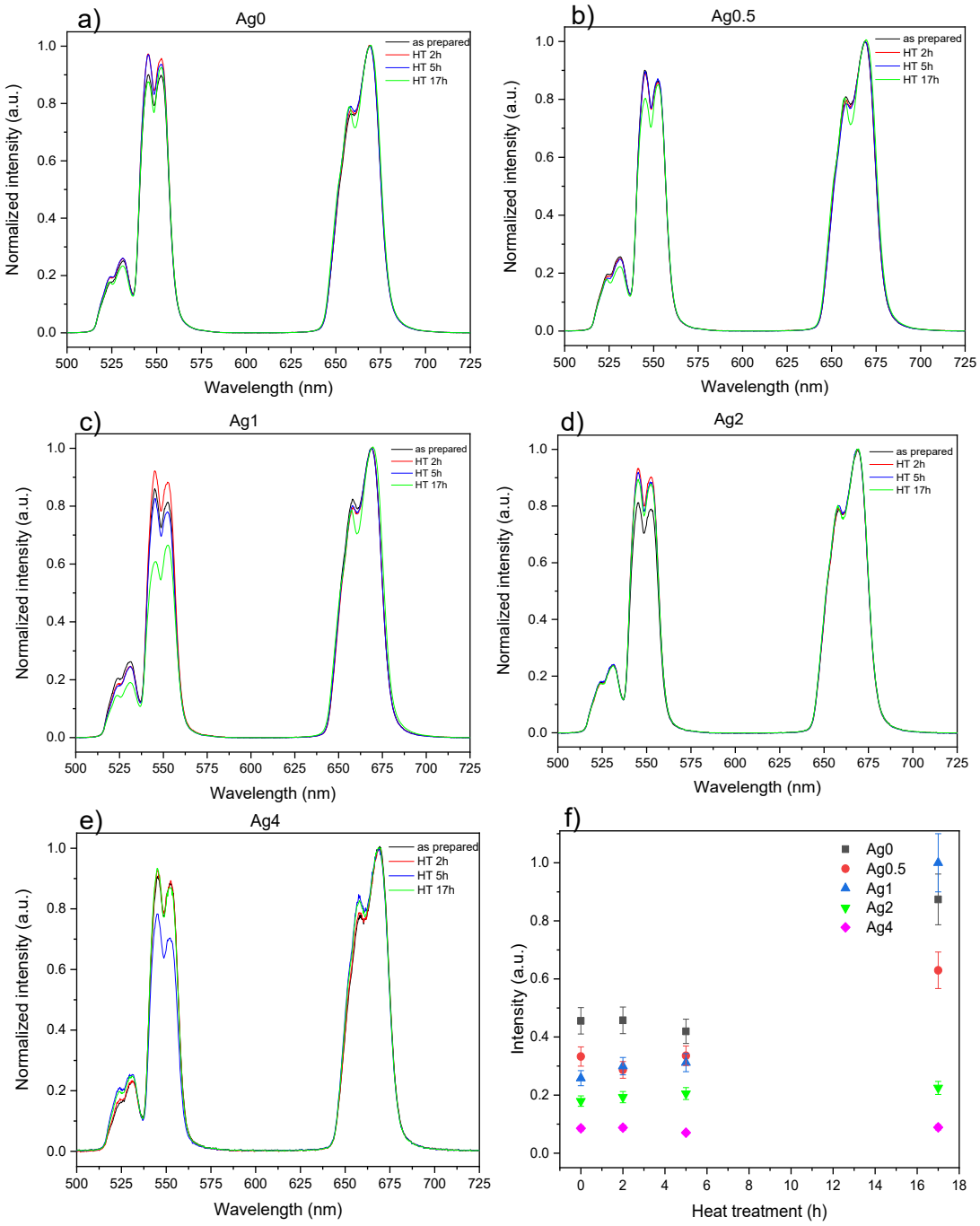

Figure 24: Normalized upconversion spectra of heat-treated glasses (a)-(e), and the intensities at 669 nm (f).

Minor modifications in the shape of the emission band can also be seen implying that the site of the Er^{3+} ions does not significantly change after heat-treatment confirming that

the sites of the Er^{3+} remain unchanged after heat treatment. As the emission bands remain broad with no appearance of sharp peaks, the Bi_4TeO_8 crystals are suspected to be Er^{3+} free.

As can be marked in Figure 24f, the intensity of the red emission from the low Ag_2O concentrated glasses increases after heat treatment for 17 h. However, as the Ag_2O content increases, the increase is less visible indicating that the increase in the intensity of the upconversion is probably related to the precipitation of Bi_4TeO_8 crystals which is less in the highly Ag concentrated glasses. It is the precipitation of the Bi_4TeO_8 crystals in the glasses with polymerized network (low Ag_2O content) which is thought to reduce the Er-Er distance increasing then the intensity of the red emission.

As shown in Figures 25, no changes in the shape and intensity of the emission at 1.5 μm were noticed for all the glasses after heat-treatment confirming that the Er^{3+} ions remain mainly in the amorphous part after heat-treatment.

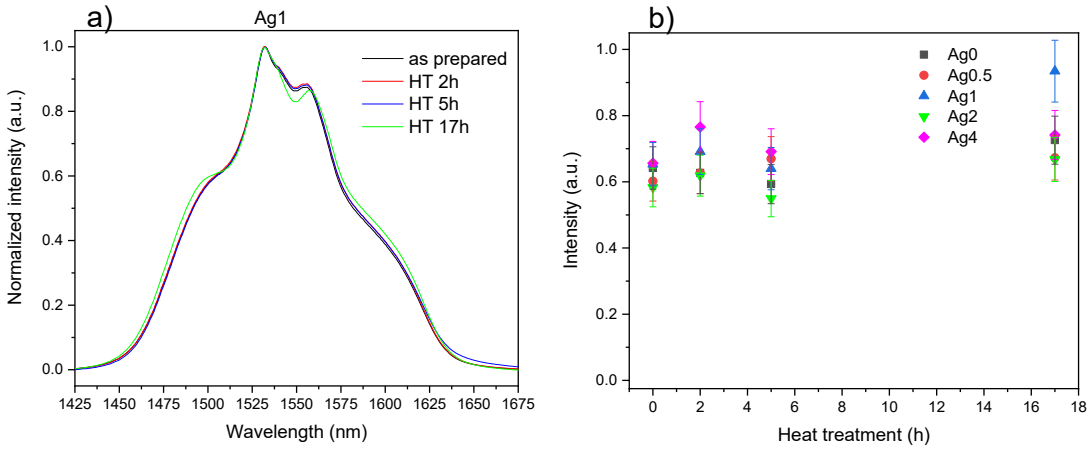

Figure 25: Normalized emission band of the Ag1 glass, taken as an example (a) and intensities at 1532 nm after heat-treatment (b).

5. CONCLUSIONS

Glasses with the composition (100-x-y) ($70TeO_2$-$20ZnO$-$10Bi_2O_3$)-xAg_2O-yEr_2O_3 with x = 0, 0.5, 1, 2 and 4 and y = 0 and 2.5 in mol% were prepared using the conventional melting quenching method. The first task of this project was to determine suitable melting conditions for Er-doped tellurite glass melted in a quartz crucible. After several trials, the melting was carried out at 775 °C for 40 minutes.

To characterize the glasses and study the impact of Ag_2O concentration on the glass thermal, physical and structural properties, the thermograms, density and Raman spectra of the glasses were measured. The addition of Ag_2O in the tellurite glass modified the glass network leading to the depolymerization of the tellurite network increasing the thermal stability while decreasing the density of the glass. Absorption spectra and luminescence measurements were used to study the effect of addition Ag_2O on the glass spectroscopic properties. Based on the absorption spectra and upconversion measurements, the addition of Ag_2O has insignificant impact on the site of the Er^{3+} ions. However, an increase in Ag_2O concentration led to a decrease in the intensity of the UC process due to depolymerization of the tellurite network increasing the Er-Er distance but did not change the intensity of the emission at 1.5 μm or the shape of emission bands. This confirmed that the sites of Er^{3+} ions are similar in all glasses and free of Ag.

In order to grow the silver nanoparticles, glasses were heat-treated at T_g + 20 °C for 2, 5 and 17 hours. The slightly pink color of the as-prepared glasses transformed first into a more orange, and finally, after 17 hours at heat-treatment, glasses were not transparent anymore. The different opacity level of the glasses depends on the Ag_2O content; due to the increase in the glass thermal stability when Ag_2O is added, the highly Ag concentrated glasses are least prone to crystallization during the heat-treatment. The crystallization was verified using XRD. The XRD pattern of the heat-treated glasses exhibit sharp peaks, which could be related to Bi_4TeO_8 crystals. No change in the shape of the emission band was observed after heat-treatment implying that the Er^{3+} ions remain in the amorphous part of the network. However, because of the precipitation of this crystals, the Er-Er distance are expected to be reduced in the polymerized glasses leading to an increase in the intensity of the upconversion. Finally, a small XRD peak observed at 38.18° might reveal the presence of Ag nanoparticles in the glasses. However, the absorption spectra exhibit no new band around 450 nm, typically related to SPR of Ag confirming that if there are Ag nanoparticles, they are probably small and/or in low concentration.

The goal of this study was to understand the impact of Ag_2O on various glass properties and to check if silver nanoparticles can be grown in the glass using heat. It was seen that tellurite glasses doped with Er^{3+} ions containing Ag_2O can be fabricated. However, no sight of the successful growth of silver nanoparticles was observed. In the future, the spectroscopic properties of the glasses can be investigated further by measuring the emission at 2.7 μm. Also, SEM coupled with EDS could be used to image and analyze the composition of the crystals to confirm that they are free of Er^{3+}.

REFERENCES

Alluxa. (2021). AZoOptics. Updated: 28.1.2021. Available: https://www.azooptics.com/Article.-aspx?-ArticleID=1178. cited 3.8.2021

Amjad, R.J., Sarah, M.R., Dousti, M.R., Ghoshal, S.K., Jamaludin, M.N.A. (2013). Surface enhanced Raman Scattering and plasmon enhanced fluorescence in zinc-tellurite glass. Optics Express. Vol.21, pp. 14282-14290. Available: https://doi.org-/10.1364/OE.21.014282.

Barbara L Dutrow, Christine M.Clark. (2020). X-ray Powder Diffraction. Available: https://serc.carleton.edu/research_education/geochemsheets/techniques/XRD.html. cited: 22.7.2021

Britannica. History of glassmaking. Available: https://www.britannica.com-/topic/glass-properties-composition-and-industrial-production-234890/History-of-glassmaking. cited: 6.8.2021

Chemistry LibreTexts. (2020). The Beer-Lambert Law. Available: https://chem.libretexts.org/Bookshelves/Physical_and_Theoretical_Chemistry_Textbook_Maps/Supplemental_Modules_(Physical_and_Theoretical_Chemistry)/Spectroscopy/Electronic_Spectroscopy/Electronic_Spectroscopy_Basics/The_Beer-Lambert_Law. cited: 9.8.2021

Da Silva, D., Kassab, L., Lüthi, S., Araújo, C., Gomes, A., Bell, M. (2007). Frequency upconversion in Er^{3+} doped $PbO\text{-}GeO_2$ glasses containing metallic nanoparticles. Applied Physics Letters vol.90. Available: https://doi.org/10.1063/1.2679798.

Dousti, M. R., Poirier, G. Y., Amjad, R. J., de Camargo, A.S.S. (2016). Luminescence quenching versus enhancement in $WO_3\text{-}NaPO_3$ glasses doped with trivalent rare earth ions and containin silver nanoparticles. Optical Materials. vol.60, pp. 331-340. Available: https://doi.org/10.1016/j.optmat.2016.08.005.

Dousti, M.R., Sahar, M.R., Ghoshal, S.K., Amjad, R.J., Arifin, R. (2013). Plasmonic enhanced luminescence in Er^{3+}: Ag co-doped tellurite glass. Journal of Molecular Structure. vol.1033, pp. 79-83. Available: http://dx.doi.org/10.1016/j.molstruc.-2012.08.022

Dousti, M.R., Sarah, M.R., Ghoshal, S.K., Amjad, R.J., Arifin, R. (2013). Plasmoinic enhances luminescence in Er^{3+}: Ag co-doped tellurite glass. Journal of Molecular Structure. vol.1033, pp. 79-83. Available: https://doi.org/10.1016/j.molstruc.2012.08.022

Edinburgh Instruments. (2021). What is Raman Spectroscopy? Updated 9.1.2021. Available: https://www.edinst.com/blog/what-is-raman-spectroscopy/. cited: 23.7.2021

Edinburgh Instruments. (2018). What is Upconversion. Available: https://www.edinst.com/blog/photon-upconversion/. cited: 4.8.2021

Epifani, M., Giannini, C., Tapfer, L., Vasanelli, L. (2000). Sol–Gel Synthesis and Characterization of Ag and Au Nanoparticles in SiO_2, TiO_2, and ZrO_2 Thin Films. Journal of the American Ceramic Society. vol.83, pp. 2385-2393.

Fares, H., Elhouichet, H., Gelloz, B., Férid, M. (2014). Silver nanoparticles enhanced luminescence properties of Er^{3+} doped tellurite glasses: Effect of heat treatment. Journal of Applied Physics. vol.116, pp.1-10. Available: https://doi.org/10.1063/1.4896363.

Fares, H., Jlassi, I., Elhouichet, H., Férid, M. (2014). Investigations of thermal, structural and optical properties of tellurite glass with WO_3 adding. Journal of Non-Crystalline Solids. vol. 396-397, pp.1-7. Available: https://www.sciencedirect.com/science/article/-pii/S0022309314001690.

Fares, H., Jlassi, I., Hraiech, S., Elhouichet, H., Férid, M. (2014). Radiative parameters of Nd^{3+}-doped titamun and tungsten modified tellurite glasses for 1.06 μm laser materials. Journal of Quantitative Spectroscopy and Radiative Transfer. vol.147, pp.224-232. Available: https://www.sciencedirect.com/science/article/pii/S0022407314002441.

FiberLabs Inc. Stimulated and spontaneous emission. Available: https://www.fiberlabs.com/glossary/stimulated-emission/.cited: 4.8.2021

lumencandela. (2016). Archimedes' Principle. Available: https://courses.-lumenlearning.com/boundless-physics/chapter/archimedes-principle/. cited: 9.8.2021

Jha, A., Richards, B., Jose, B.D.O.,Toney Fernandez, T., Hill, C.J., Lousteau, J., Joshi, P. (2012). Review on structural, thermal, optical and spectroscopic properties of tellurite oxide based glasses for fibre optic and waveguide. Int. Mater. Rev. vol.57, pp.357-382. Available: http://dx.doi.org/10.1179/1743280412Y.0000000005 .

Jiang, Y., Fan, J., Jiang, B., Mao, X., Tang, J., Xu, Y., Dai, S., Zhang, L. (2016). Er^{3+}-doped transparent glass ceramics containing micro-sized SrF_2 crystals for 2.7 μm emissions. Scientific reports. vol.6, pp.1-7, Available: http://dx.doi.org/10.1038/-srep29873.

Jlassi, I., Elhouichet, H., Ferid, M. (2011). Thermal and optical properties of tellurite glasses doped erbium. Journal of Material Science. vol.46, pp. 806-812. Available: https://link.springer.com/article/10.1007/s10853-010-4820-x.

Kaur, A., Khanna, A., Pesquera, C., González, F., Sathe, V. (2010). Preparation and characterization of lead and zinc tellurite glasses. Journal of Non-Crystalline Solids.

vol.356, pp.864-872. Available: https://www.sciencedirect.com/science/article/pii/-S00223093-10000153.

Kemere, M., Sperga, J., Rogulis, U., Krieke, G., Grube, J. (2017). Luminescence properties of Eu, RE^{3+} (RE = Dy, Sm, Tb) co-doped oxyfluoride glasses and glass–ceramics. Journal of Luminescence. vol.181, pp. 25-30. Available: https://www.sciencedirect.com/science/article/pii/S0022231316305385.

Liu, L., Sun, Z., Ma, C., Tao, R., Zhang, J., Li, H., Zhao, E. (2018). Higly sensitive and accurate optical thermometer through Er doped tellurite glasses. Materials Research Bulletin. vol.105, pp. 306-311, Available: https://doi.org/10.1016/j.mater-resbull.2018.04.053.

Mahraz, Z. A. S., Sahar, M.R., Ghoshal, S.K., Dousti, M.R., Amjad, R.J. (2013). Silver nanoparticles enhanced luminescence of Er^{3+} ions in boro-tellurite glasses. Material Letters. vol.112, pp. 136-138. Available: https://doi.org/10.1016/j.matlet.2013.08.131.

Mahraz, Z.A.S., Sarah, M.R., Ghoshal, S.K. (2015). Enhance luminescence from silver nanoparticles integrated Er^{3+}-doped boro-tellurite glasses: Impact of annealing temperature. Journal of Alloys and Compounds. vol.649, pp. 1102-1109. Available: https://doi.org/10.1016/j.jallcom.2015.07.232.

Massera, J., Haldeman, A., Jackson, J., Rivero-Baleine, C., Petit, L., Richardson, K. (2010). Processing of Tellurite-Based Glass with Low OH Content. Journal of the American Ceramic Society. vol.94, pp. 130-136. Available: https://doi.org/10.1111/j.-1551-2916.2010.04031.x.

Massera, J., Remond, J., Musgraves, J., Davis, M.J., Misture, S., Petit, L., Richardson, K. (2010). Nucleation and growth behavior of glasses in the TeO_2–Bi_2O_3–ZnO glass system. Journal of Non-Crystalline Solids. vol.356, pp. 2947-2955. Available: https://doi.org/10.1016/j.jnoncrysol.2010.03.045.

Nissink Business Glass. History of Glass. Available: http://www.nissinkglass.co.-uk/info/history-of-glass. cited: 6.8.2021

Petit, L., Cardinal, T., Videau, J.J., Le Flem, G., Guyot, Y., Boulon, G., Couzi, M., Buffeteau, T. (2002). Effect of the introduction of $Na_2B_4O_7$ on erbium luminescence in tellurite glasses. Journal of Non-Crystalline Solids. vol.298, pp. 76-88. Available: http://dx.doi.org/10.1016/S0022-3093(01)01036-5

Pugliese, D., Boetti, N. G., Lousteau, J., Ceci-Ginistrelli, E., Bertone, E., Geobaldo, F., Milanese, D. (2016). Concentration quenching in an Er-doped phosphate glass for compact optical lasers and amplifiers. Journal of Alloys and Compounds. vol.657, pp. 678-683. Available: https://doi.org/10.1016/j.jallcom.2015.10.126.

Qi, J., Xu, T., Wu, Y., Shen, X., Dai, S., Xu, Y. (2013). Ag nanoparticles enhanced near-IR emission from Er^{3+} ions doped glasses. Optical Materials. vol.35, pp. 2502-2506. Available:https://www.sciencedirect.com/science/article/pii/S0925346713003765#!

Qi, Y., Zhou, Y., Wu, L., Yang, F., Peng, S., Zheng, S., Yin, D. (2014). Silver nanoparticles enhanced 1.53 μm band fluorescence of Er^{3+}/Yb^{3+} codoped tellurite glasses. Journal of Luminescence. vol.153, pp. 401-407. Available: https://doi.org/10.1016/-j.jlumin.2014.03.069.

Schweizer, T., Brady, D.J., Hewak, D.W. (1997). Fabrication and spectroscopy of erbium doped gallium lanthanum sulphide glass fibers for mid-infrared laser applications. Optics Express. vol.1, pp. 102-107. Available: https://doi.org/10.1364/OE.1.000102.

Sekiya, T., Mochida, N., Ohtsuka, A., Tonokawa, M. (1992). Structural study of MoO_3TeO_2 glasses. Non-Crystalline solids. vol.185, pp.135-144.

Shameli, K., Ahmad, M.B., Zamanian, A., Sangpour, P., Shabanzadeh, P., Abdollahi, Y., Zargar, M. (2012). Green biosynthesis of silver nanoparticles using Curcuma longa tuber powder. International Journal of Nanomedicine. vol. 7, pp. 5603-5610. Available: https://www.dovepress.com/ by 130.230.124.55.

Shelby, J. E. (2005). Introduction to Glass Science and Technology. 2nd. Cambridge: The Royal Sosiety of Chemistry.

Shen, X., Zhang, Y., Xia, L., Li, J., Yang, G., Zhou, Y. (2020). Broadband flat near-infrared emission from tellurite glass doped with Tm^{3+}, Er^{3+} and Ag NPs. Optics and Laser Technology. vol.129, pp.1-11. Available: https://doi.org/10.1016/j.optlastec.-2020.106264.

Simo, A., Polte, J., Pfänder, N., Vainio, U., Emmerling, F., Rademann, K. (2012). Formation Mechanism of Silver Nanoparticles Stabilized in Glassy Matrices. Journal of the American Chemical Society. vol.134, pp. 18824-18833.

Solé, J.G., Bausá, L.E., Jaque, D. (2005). An intorduction to the Optical Spectroscopy of Inorganic Solids. John Wiley & Sons. pp.1-38.

Stambouli, W., Elhouichet, H., Gelloz, B., Férid, M., Koshida, N. (2012). Energy transfer induced Eu^{3+} photoluminescense enhancement in tellurite glass. Journal of Luminescence. vol.132, pp. 205-209. Available: https://www.sciencedirect.com/-science/article/pii/S0022231311004650.

Swetha, B.N., Devarajulu, G., Keshavamurthy, K., Jagannath, G., Deepa, H.R. (2021). Enhanced 1.53 μm emission of Er^{3+} in nano-Ag embedded sodium-boro-lanthane glasses. Jornal of Alloys and Compounds. vol.856, pp.1-9. Available: https://doi.org/10.1016/j.jallcom.2020.158212.

Synopsys. (2021). Photonics. Available: https://www.synopsys.com/glossary/what-is-photonics.html. cited: 7.9.2021

Yusoff, N.M., Sahar, M.R. (2015). Effect of silver nanoparticles incorporated with samarium-doped magnesium tellurite glasses. Physica B: Condensed Matter. vol.456, pp. 191-196. Available: https://doi.org/10.1016/j.physb.2014.08.039.

xrd.co. Every thing you want to know about X-Ray Diffraction. Available: https://xrd.co/component-parts-x-ray-diffractometer/. cited 25.7.2021